Exploring the Tully-Fisher Relationship Using Online Databases

Chris Williams
Student 1607421
HET 604

13th June 2002

Introduction

One of problems that has dogged the science of astronomy from it inception is that of determining how far away objects are. Astronomers have devised a range of tools to convert from things we can measure into distances. One of the most easily measured attributes of an object is its brightness. The difference between how bright an object in the sky appears (apparent brightness) and how bright it actually is (absolute brightness) can be used to determine distance using an simple relationship. For certain types of object, called standard candles, it is possible to determine how bright the object actually is, allowing a distance calculation to be made. Amongst these objects are Cepheid variable stars and Type Ia supernovae. Cepheid stars are visible over very large distances and can be seen in nearby galaxies, while supernovae can be seen over immense distance but are far more rare. For the vast majority of galaxies though, no standard candles are available and the distance remains unknown. Coarse estimates of distance can be made using measurement of cosmological recession and the Hubble constant, the value of which is still quite uncertain, or cluster studies. Distances derived from less certain sources can be verified if a second, independent measurement method is available. The Tully-Fisher relation is one such method.

This project aims to investigate the Tully-Fisher relation in general. A sample Tully-Fisher relation will be constructed for different morphological types using data from the Lyon-Meudon Extra-galactic Database (LEDA) and the ATNF HIPASS online databases.

Tully-Fisher Relation

Brent Tully and Richard Fisher [1] provided details of a secondary mechanism for distance determination of spiral galaxies in 1977. The Tully-Fisher relation, as it is now known, relates rotation speed, a distance independent measurable property, and absolute magnitude. The precise mechanism driving the relationship is not fully understood but it is essentially a correlation between mass and luminosity. The rotation velocity of the galaxy determines the mass contained within the orbit: more mass equates to more stars and therefore luminosity.

The Tully-Fisher relation is usually quoted in the form:

$$M = a(\log W_{20}^{i} - 2.5) + b \tag{1}$$

where M is absolute magnitude, W_{20}^{i} is the width of the H I line as as discussed below, and x and y are coefficients determined by fitting to observational data. The b value gives the absolute magnitude for $W \simeq 320$ km s^{-1}, and a the slope of the curve.

Measuring Rotation

Galactic rotation is measured by observing the spread of emission lines due to Doppler effects. In Tully and Fisher's work the 21 cm emission line of neutral, atomic hydrogen (H I) was used for this purpose. Neutral hydrogen is a tracer for spiral arms in galaxies and, in general, extends much further than the visible portions of a galaxy would indicate. Th H I emission line is a good choice because it is largely unaffected by absorption and scattering en-route from the galaxy being observed.

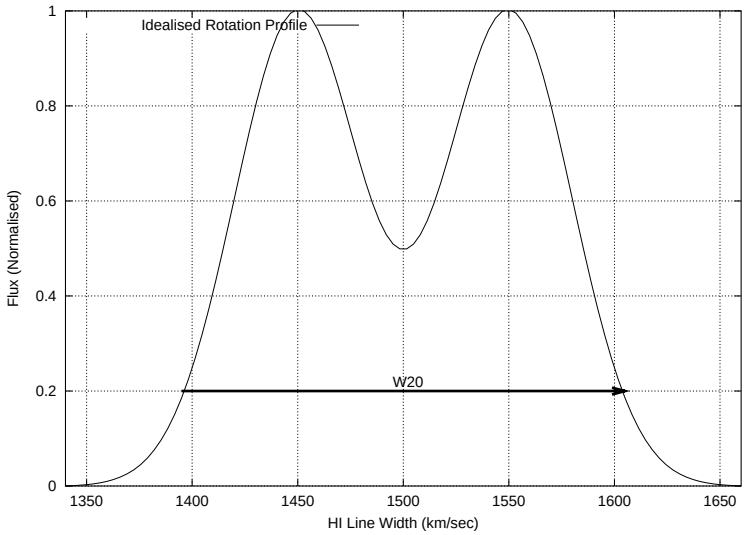

Figure 1: Measurement of the H I line width is usually made at 20% of the peak emission. The figure is expressed in km s^{-1} and must be corrected for inclination of the galaxy to our line of sight.

H I line width (W_{20}) is generally measured at 20% of the peak value for the emission line as depicted in Figure 1. The measured value must be adjusted, Equation 2, to account for the effects of galaxy inclination (i) to arrive at the value (W_{20}^{i}) for a perfectly edge on galaxy.

$$W_{20}^{i} = \frac{W_{20}}{\sin i} \tag{2}$$

Variation with Observation Band

Tully and Fisher used B-band photographic magnitudes of local galaxies to calibrate their relation. For galaxies at greater distance or obscured by galactic

dust B-band photometry may not be optimal. Consequently photometry in other bands, particularly near IR (I-band) but also V, R, K and H-bands, is used for much of the detailed work with Tully-Fisher relations. Subsequent investigations have shown that, while the Tully-Fisher relation holds in other observation bands, the coefficients vary. Typical values for Tully-Fisher relations in five bands as given in Sakai *et al* [2] are:

$$\begin{aligned} B_T^c &= (7.97 \pm 0.72)(\log W_{20}^c - 2.5) - (19.80 \pm 0.11) \\ V_T^c &= (8.87 \pm 0.83)(\log W_{20}^c - 2.5) - (20.34 \pm 0.12) \\ R_T^c &= (8.78 \pm 0.72)(\log W_{20}^c - 2.5) - (20.65 \pm 0.11) \\ I_T^c &= (9.24 \pm 0.75)(\log W_{20}^c - 2.5) - (21.12 \pm 0.12) \\ H_{-0.5}^c &= (11.03 \pm 0.86)(\log W_{20}^c - 2.5) - (21.74 \pm 0.14) \end{aligned} \tag{3}$$

Extinction Corrections

Before a distance determination can be made using the Tully-Fisher relation the apparent magnitude of the target galaxy must determined in the observation band of choice. The measured magnitude must be corrected for a number of factors:

- Extinction due to intergalactic dust. This is a minor correction and can usually be omitted unless there are known obscuring agents such as dense intra-cluster gas and dust.
- Extinction due to galactic dust. Extinction of light by dust within the plane of the Milky Way can be quite extreme. Detailed maps of H I and dust distribution within the galaxy can be used to correct for this source of extinction. However, near the galactic plane these corrections have large uncertainties so Tully-Fisher surveys are generally limited to mid to high galactic latitudes [3].
- Self-extinction. The dust and gas of a galaxy also reduce its own apparent luminosity by obscuring light from 'rear-ward' portions of the galaxy. This extinction is discussed in more detail below.

Tully and Fisher used a basic correction for self-extinction due to inclination from Sandage and Tamman [4] : $A_i = 0\overset{m}{.}28(a/b - 1)$ where a and b are the observed major and minor axes of the galaxy. Far more detailed assessments of this phenomenon have been undertaken since 1977 to arrive at a set of statistically based corrections. A typical result from Tully *et al* [5] is:

$$A_i = \gamma \log(a/b) \tag{4}$$

where γ is a multiplier derived for a given observation band and rotation rate:

$$\begin{aligned} \gamma_B &= 1.57 + 2.75(\log W_R^i - 2.5) \\ \gamma_R &= 1.15 + 1.88(\log W_R^i - 2.5) \\ \gamma_I &= 0.92 + 1.63(\log W_R^i - 2.5) \end{aligned}$$

Variation with Morphology

The Tully-Fisher relation is targeted at spiral galaxies. The use of H I as a gauge of rotation is impacted by the amount and concentration of neutral hydrogen present. Infrared telescope surveys of galaxies show that Sa galaxies are approximately 4% gas and dust by mass, Sb and Sc are 8% and 25% respectively [6, §26.3]. The distribution of matter in Sa galaxies is more central, with smaller spiral structures, than that of Sc spirals. Consequently, the H I emission from Sa galaxies may under-represent the maximum rotation rate because there is little gas in the outer regions. It seems reasonable, therefore, to expect variation between a Tully-Fisher relation derived using spirals of differing morphology.

Another effect of morphology relates to low-luminosity spirals and irregular galaxies. If Tully-Fisher relations are to be applied to these galaxy types then more complex consideration of the H I profile width is required. The assumption of $W_{20} \approx 2V_{max}$ fails because of internal turbulence and H I line profile factors. For $W^i_{20} > 150$km s^{-1} these effects are negligible [3].

Data Collection

Data Sources

Lyon-Meudon Extragalactic Database (LEDA). The LEDA is a repository for homogenised observational data of extra-galactic objects. Created in 1983 at the Lyon Observatory, and maintained ever since, the database hold records for approximately 1.06 million objects. The range of parameters available for any object is quite extensive. For this project only the identifying number, location in equatorial and galactic coordinates, recession velocity, inclination, photographic (B) magnitude, galactic extinction, morphological type, major to minor axis ratio, and multiple galaxy flag are directly used. Other values, such as absolute magnitude, H I line width, and inclination correction, were used only as a check for gross errors.

H I Parkes All-Sky Survey (HIPASS). The Parkes radio-telescope has been used to carry out a survey of the entire southern sky at 21cm wavelengths. The Parkes telescope is part of the Australia Telescope which is funded by the Commonwealth of Australia for operation as a National Facility managed by CSIRO. The spectral data has been reduced (Barnes *et al* [7]), and one dimensional spectra, in various formats, have been made available to the public through their WWW site. This project makes use of spectra for several hundred objects in FITS format.

Sample Selection

As a starting point, an extract of key data for 2696 galaxies in the relatively near regions ($500 < \mathrm{v}_{recession} < 2000$ kms^{-1}) was extracted from the LEDA database. This recession velocity range was chosen to:

- avoid confusion of the target galaxy's profile with the very strong HI signals from Milky Way sources;

- avoid a potential source of interference in the HIPASS data from the 11th harmonic of the 128 MHz sampler clock at 1408 MHz, or $cz = 2640$ kms^{-1}; and
- keep the sample numbers to a manageable size.

Of all the galaxies represented in the LEDA extract only a subset are suitable for development of a Tully-Fisher relation. The selection criteria applied to find a suitable subset were:

- Known morphological type on either S or SB branch of Hubble classification scheme. Elliptical (E), lenticular (SO and SBO), Magellanic (Sm) and irregular (Irr) morphological types are excluded.
- Known inclination greater than 45°, after Tully and Fisher [1], to minimise effects of correcting the rotation profile for inclination.
- Apparent magnitude (B-band) known. The LEDA value has been standardised during the catalogue compilation using methods described by Paturel *et al* [8]. These values are used without alteration.
- Southern declination so that HIPASS data is available for the object.
- Galactic latitude greater than 30° so that galactic extinction, and its uncertainty, is minimal. LEDA quotes galactic extinction figures derived from Schlegel, Finkbeiner and Davis [9] which will be used as-is.
- Not a multiple galaxy to avoid confusion in HI profiles.
- Not a member of a Lyon galaxy group as defined by Garcia [10] and amendments within the LEDA database. Intra-cluster peculiar motions have the potential to distort calculation of the absolute magnitude because recession velocity, a compound of Hubble expansion and galaxy motion, is used to determine the distance modulus. This restriction removes many galaxies but also removes uncertainty associated with clusters.

Galaxies that survived the filtering process were split into two groups for further analysis:

- Early. Morphological types Sa, Sab, Sb, Sbc, SBa, SBab, SBb, SBbc.
- Late. Morphological types Sc, Scd, Sd, SBc, SBcd, SBd.

Table 1 shows a summary of the selection process.

Rotation Velocity Determination

The HIPASS database was queried for H I flux versus velocity plots for the targets. Data was retrieved for a velocity range of -1281 to 2500 kms^{-1} in unsmoothed, one-dimensional FITS format. HIPASS data is delivered with the continuum subtracted so that the spectra are zero based. In some spectra a residual 5MHz ripple due to equipment characteristics is evident.

The IRAF *splot* task was used to analyse these spectra. Initial approaches using *splot* to fit Gaussian distributions to the H I peaks proved unsatisfactory

Total in extract	2696
Exclusions	
North of celestial equator	1669
Too close to galactic plane	563
Inclination too small	667
Multiple galaxy	143
Non-spiral morphology	1305
LGG galaxy	1010
Total kept	165
Early morphology	58
Late morphology	107

Table 1: Summary of selection process. Note that some galaxies will be counted in several exclusion groups.

given the wide range of peak shapes and the poor fit to the majority of these peaks. Fitting multiple Gaussians to each target spectra was tried but found to be cumbersome and of dubious consistency. No other IRAF task seemed more suited to the process of fitting a curve to multi-peak spectra so a more basic approach was adopted. Analysis of each galaxy consisted of:

- Loading the spectra into *splot*.
- Locating the target galaxy along the velocity axis.
- Expanding the region surrounding the target so the peak of interest occupied the majority of the display, providing the best possible horizontal resolution.
- Measuring the velocity at both extremes of the peak where the flux dropped back to zero. In cases where the flux did not return to zero, due to noise, extended tails, or a non-zero continuum, an approximation was made by projecting the main downward flux curve to the zero baseline.
- Calculate the recession velocity as the average of upper and lower bounds.
- Calculate the rotation profile width as the difference between the upper an lower bound.
- Correct the profile width for inclination using Equation 2 and the LEDA supplied inclination.

The adopted method for measuring the rotation width differs from the methods used by Tully, Fisher and others. Generally, the rotation curve width is measured at 20% of the peak flux giving the value W_{20} seen in the literature. Had the Gaussian fit approach been suitable, the width at 20% would have been derivable from the standard Gaussian full width at half maximum. The simpler approach measures a wider portion of the curve and suffers greater uncertainties from noise and curve tail effects. Given the higher rotation velocities obtained using this method, it is expected that any derived Tully-Fisher relationship will have a lower slope than those found in published literature.

Comparison of measured values against values recorded by LEDA indicate that only one of the measured centre velocities varies by more than ±5%. Measured rotation velocities are not directly comparable between this study and LEDA. Inspection shows 11 calculated H I line widths are up to 5% smaller than the equivalent LEDA value, but generally, the calculated value is higher (average ∼18%).

Of the candidate galaxies 17 early and 17 late types were not measurable for one of the following reasons:

- No discernible spectral peak could be found.
- A peak was found, but it was not close to the recession velocity expected for the target.
- A weak signal was found but the signal to noise ratio made defining its boundaries uncertain.
- In one case, the upper end of the rotation curve fell outside the extracted velocity range.

The velocity resolution of the HIPASS data is 18 kms^{-1}. The *splot* task plots this data with a straight line interpolation between samples. In *splot* measurements are made to the nearest interpolated pixel. Typically, a variation of a few pixels either side of the exact zero crossing could be expected during measurement, an error estimated at ±15 kms^{-1}. The derived centre and rotation velocities will carry an uncertainty of ±21 kms^{-1} as a result. Table 2 shows the results.

Absolute Magnitude Calculation

Prior to absolute magnitude calculation, the apparent magnitude (m) must be corrected for inclination induced self-extinction. For this purpose, Equation 4 and the B-Band γ value were used, with the corrected, measured profile width in place of W_{20} and LEDA supplied base magnitude and major to minor axis ratio. The calculated corrections (A_i) were in general agreement with figures published by LEDA. The higher value and uncertainty of profile width measurements carries through into a slightly larger and less certain magnitude adjustment.

Corrections for galactic extinction (A_g) were adopted directly from LEDA. Distances were calculated using the measured recession velocity and an assumed Hubble constant of 75 Mpc/kms^{-1}.

The corrected apparent magnitude (m_c) and absolute magnitude (M) were calculated:

$$\begin{aligned} m_c &= m_B - A_g - A_i \\ M &= m_c - 5\log(d) + 5 \end{aligned}$$

The base LEDA photographic magnitude carries a standard deviation, where quoted, of between 0.06 and 1.27 magnitudes. The logarithm of the major to minor axis ratio is given a deviation varying from 0.03 to 0.48. No tolerances are given on galactic extinction or inclination. The measured rotation velocity and recession velocity are used in calculation of the absolute magnitude, so

those errors are considered. Error propagation was calculated using formulae from University of Michigan [11]. Results are shown as error bars on the data plots shown later, and in Table 2. The maximum standard deviation is 1.28 magnitudes, and the median is 0.27.

Analysis and Discussion

For each morphological group a curve was fit to the profile width and absolute magnitude data. The plotting tool (gnuplot) uses an implementation of the nonlinear least-squares (NLLS) Marquardt-Levenberg algorithm and was asked to fit a function of the form shown in Equation 1. Only estimated absolute magnitude error estimates are used in the fitting process: rotation velocity error estimates are constant and would not affect the fit. The resulting plots are shown in Figures 2 and 3, with both fits shown in Figure 4. The values of the fit coefficients are summarised in equations 5 and 6.

$$M_{early} = (-7.40 \pm 0.88)(\log W - 2.5) - (-19.19 \pm 0.12) \quad (5)$$

$$M_{late} = (-6.85 \pm 0.51)(\log W - 2.5) - (-19.49 \pm 0.09) \quad (6)$$

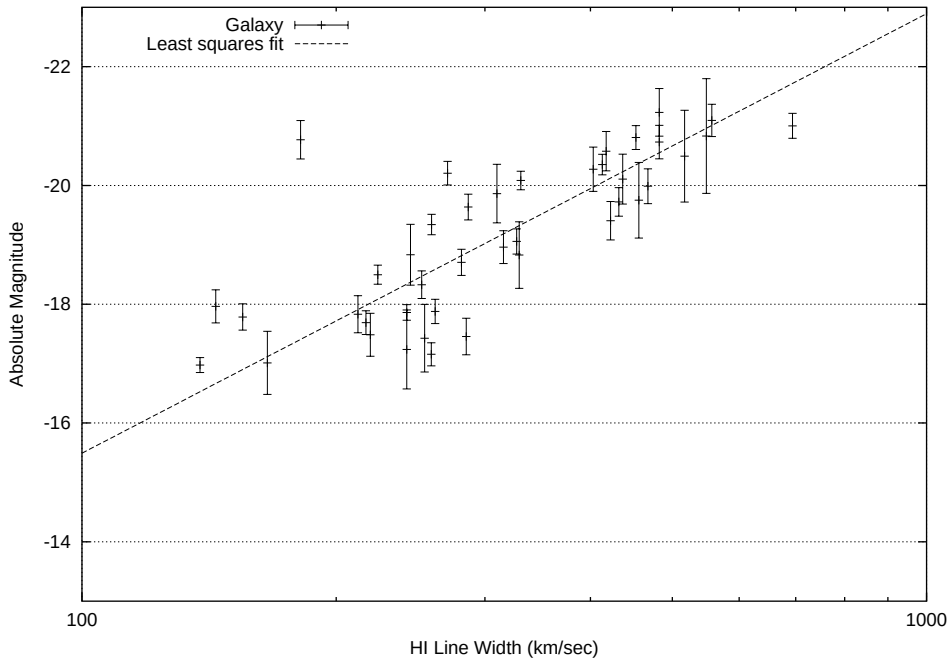

Figure 2: Tully-Fisher plot for early morphological types.

The plots show a definite relationship between rotation velocity and absolute magnitude with surprisingly few outliers. This result is in general agreement with that of Tully and Fisher.

The derived relation slopes are lower than the typical values of Equation 3. As discussed earlier, the measurement method's increased velocity will be shallowing the slope. Early morphological groups show a steeper slope than the late

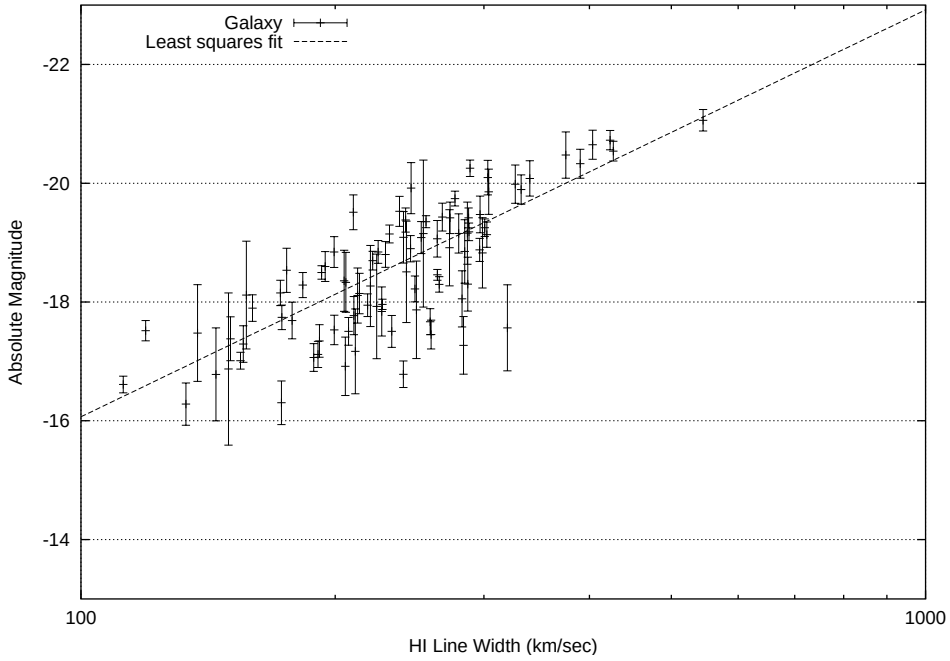

Figure 3: Tully-Fisher plot for late morphological types.

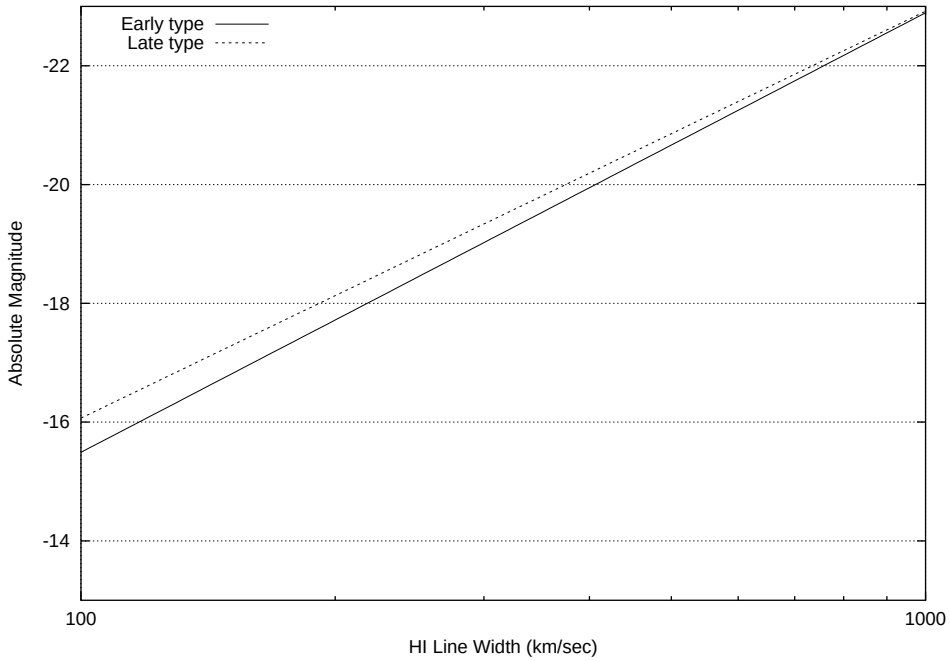

Figure 4: Fit lines overlaid for comparison.

types. Visual inspection of the plots does not indicate a substantially different closeness of fit.

The intercept values are close to each other. In comparison to the relation of equation 3, the base magnitude is 0.3 to 0.6 magnitudes dimmer. This discrepancy may be partly accounted for by the inclination correction for self-extinction, which is sensitive to the width measurement and expected to add $\sim$0.2 to the γ calculation based on an estimated 1.2$\times$ greater line width.

The scatter of galaxies about the fit lines is quite broad. The variance of residual values produced by the fitting algorithm, both approximately 8, may indicate incorrect data error estimates, that data errors not normally distributed, systematic measurement errors, or aberrant outliers. Measurement of line widths would be the most likely substantial source of error and this is weakly coupled into the absolute magnitude variance. Proper motion of the sample galaxies could also contribute to skew in the absolute magnitude figures.

The plots reveal a skew in H I line width: the late types rotating more slowly, on average, than the early types. This is consistent with the differing distribution of neutral hydrogen within the galaxies discussed earlier (pp. 4).

Conclusion

The sample studied clearly shows a relationship between rotation velocity and absolute magnitude. This relationship is evident even using rough measurement techniques for the H I profile width. There's a small difference between the relations for early and late morphological types.

The Tully-Fisher relation would make a useful tool for obtaining order-of-magnitude estimates of distance to galaxies for which a more specific tool, such as Cepheid or Ia supernova measurements, is available.

Acknowledgements. Data from the LEDA database (`http://leda.univ-lyon1.fr`) has been used in this project. Data from the ATNF HIPASS survey has been used in this project. The Parkes telescope is part of the Australia Telescope which is funded by the Commonwealth of Australia for operation as a National Facility managed by CSIRO.

		LEDA Supplied					Measured		
PCG	Name	Morphology	Inclination	Apparent Magnitude	Galactic Extinction	Log a/b	Centre Velocity	Line Width	Absolute Magnitude
50229	MCG0-36-18	Sa	63.6	14.70 (0.25)	0.26	0.28 (0.05)	1601.3 (21.2)	285.1 (21.2)	-17.5 (0.31)
14818	NGC1556	Sab	79.3	13.57 (0.19)	0.09	0.48 (0.05)	984.4 (21.2)	216.9 (21.2)	-17.7 (0.20)
13998	ESO359-3	Sab	82.9	14.13 (0.27)	0.04	0.48 (0.07)	1548.8 (21.2)	144.0 (21.2)	-18.0 (0.28)
12559	NGC1306	Sb	48.3	14.50 (0.49)	0.07	0.16 (0.08)	1447.5 (21.2)	242.4 (21.2)	-17.2 (0.66)
11744	MCG-2-9-2	Sb	67.8	14.60 (0.20)	0.3	0.35 (0.06)	1556.0 (21.2)	155.0 (21.2)	-17.8 (0.22)
54364	NGC5878	Sb	69	12.51 (0.28)	0.61	0.37 (0.05)	1973.2 (21.2)	482.6 (21.2)	-20.7 (0.28)
71716	NGC7690	Sb	70.1	13.22 (0.56)	0.05	0.38 (0.05)	1481.2 (21.2)	329.4 (21.2)	-18.8 (0.56)
72163	MCG-2-60-13	Sb	75.4	15.79 (0.11)	0.15	0.44 (0.12)	1907.2 (21.2)	138.0 (21.2)	-17.0 (0.13)
13211	ESO548-43	Sb	80.4	15.77 (0.16)	0.15	0.51 (0.14)	1951.6 (21.2)	259.2 (21.2)	-17.2 (0.19)
52507	NGC5729	Sb	87.7	12.99 (0.10)	0.36	0.59 (0.07)	1802.0 (21.2)	330.9 (21.2)	-20.1 (0.16)
14071	NGC1484	Sb	90	13.87 (0.31)	0.06	0.69 (0.09)	1040.6 (21.2)	212.2 (21.2)	-17.8 (0.31)
70565	ESO469-15	Sb	90	15.02 (0.12)	0.12	0.82 (0.13)	1626.5 (21.2)	242.4 (21.2)	-17.9 (0.13)
15455	ESO202-35	Sb	90	13.23 (0.49)	0.05	0.81 (0.07)	1860.2 (21.2)	310.0 (21.2)	-19.9 (0.49)
13586	NGC1433	SBa	49	10.77 (0.16)	0.04	0.16 (0.16)	1067.2 (21.2)	271.0 (21.2)	-20.2 (0.20)
69521	IC5240	SBa	58	12.68 (0.21)	0.07	0.22 (0.06)	1731.4 (21.2)	422.5 (21.2)	-19.4 (0.32)
45596	NGC4980	SBa	71.8	13.49 (0.07)	0.31	0.35 (0.05)	1414.1 (21.2)	224.0 (21.2)	-18.5 (0.16)
13434	NGC1398	SBab	45.7	10.54 (0.14)	0.06	0.14 (0.03)	1373.7 (21.2)	693.9 (21.2)	-21.0 (0.21)
9747	NGC986	SBab	57.4	11.70 (0.17)	0.08	0.23 (0.15)	1962.7 (21.2)	181.5 (21.2)	-20.8 (0.32)
38580	NGC4129	SBab	90	13.19 (0.20)	0.31	0.55 (0.05)	1164.1 (21.2)	281.4 (21.2)	-18.7 (0.22)
2437	NGC210	SBb	53.7	11.80 (0.37)	0.09	0.20 (0.04)	1628.0 (21.2)	403.0 (21.2)	-20.3 (0.37)
53417	NGC5781	SBb	59	13.84 (0.14)	0.42	0.25 (0.05)	1893.6 (21.2)	315.6 (21.2)	-19.0 (0.28)
35097	NGC3673	SBb	59.9	12.55 (0.28)	0.24	0.26 (0.10)	1906.9 (21.2)	436.8 (21.2)	-20.1 (0.42)
2052	NGC150	SBb	63.9	12.12 (0.23)	0.06	0.31 (0.05)	1557.9 (21.2)	467.9 (21.2)	-20.0 (0.29)
7544	NGC779	SBb	73.7	12.27 (0.63)	0.12	0.43 (0.09)	1365.4 (21.2)	456.4 (21.2)	-19.8 (0.64)
7262	NGC755	SBb	78.2	13.15 (0.16)	0.1	0.50 (0.05)	1619.8 (21.2)	259.4 (21.2)	-19.3 (0.17)

		LEDA Supplied					Measured		
PCG	Name	Morphology	Inclination	Apparent Magnitude	Galactic Extinction	Log a/b	Centre Velocity	Line Width	Absolute Magnitude
53499	NGC5792	SBb	82.2	12.52 (0.75)	0.25	0.54 (0.12)	1904.3 (21.2)	517.1 (21.2)	-20.5 (0.77)
5849	NGC613	SBbc	46.9	10.99 (0.77)	0.08	0.18 (0.16)	1464.5 (21.2)	548.5 (21.2)	-20.8 (0.97)
2492	MCG-3-2-40	SBbc	49.6	14.12 (0.16)	0.12	0.17 (0.03)	1558.3 (21.2)	262.0 (21.2)	-17.9 (0.20)
2081	NGC157	SBbc	55.2	11.05 (0.32)	0.19	0.22 (0.06)	1663.8 (21.2)	482.5 (21.2)	-21.2 (0.40)
13999	IC2051	SBbc	55.5	11.82 (0.18)	0.49	0.22 (0.03)	1700.2 (21.2)	452.8 (21.2)	-20.8 (0.20)
33550	NGC3521	SBbc	65.5	9.73 (0.24)	0.25	0.30 (0.07)	783.9 (21.2)	556.9 (21.2)	-21.1 (0.27)
37318	ESO572-12	SBbc	70.1	15.53 (0.12)	0.18	0.40 (0.23)	1650.5 (21.2)	165.8 (21.2)	-17.0 (0.53)
69253	NGC7314	SBbc	70.3	11.68 (0.11)	0.09	0.38 (0.04)	1391.1 (21.2)	413.1 (21.2)	-20.4 (0.17)
70324	NGC7462	SBbc	90	13.02 (0.50)	0.05	0.71 (0.12)	1051.2 (21.2)	244.9 (21.2)	-18.8 (0.51)
68389	IC5176	SBbc	90	13.43 (0.20)	0.13	0.82 (0.14)	1704.7 (21.2)	432.2 (21.2)	-19.7 (0.24)
12979	NGC1345	SBc	45.4	14.29 (0.18)	0.16	0.14 (0.06)	1529.8 (21.2)	259.1 (21.2)	-17.7 (0.22)
36885	ESO504-17	Sbc	45.4	15.14 (0.56)	0.38	0.14 (0.08)	1847.8 (21.2)	254.5 (21.2)	-17.4 (0.57)
70184	IC5273	SBc	51.3	12.73 (0.59)	0.05	0.19 (0.03)	1283.8 (21.2)	298.8 (21.2)	-18.8 (0.59)
71729	NGC7689	SBc	51.5	12.13 (0.07)	0.05	0.20 (0.04)	1944.8 (21.2)	390.1 (21.2)	-20.3 (0.24)
5619	NGC578	SBc	56.1	11.60 (0.19)	0.05	0.21 (0.09)	1607.0 (21.2)	375.1 (21.2)	-20.5 (0.39)
14814	NGC1559	SBc	58.2	11.01 (0.13)	0.13	0.26 (0.04)	1271.0 (21.2)	423.1 (21.2)	-20.7 (0.16)
68128	NGC7205	Sbc	60.3	11.70 (0.26)	0.1	0.27 (0.09)	1669.0 (21.2)	417.4 (21.2)	-20.6 (0.33)
46126	NGC5042	SBc	60.4	12.48 (0.27)	0.78	0.28 (0.03)	1374.4 (21.2)	303.2 (21.2)	-20.1 (0.29)
44952	MCG-2-33-93	SBc	60.6	14.01 (0.08)	0.24	0.28 (0.03)	1333.9 (21.2)	227.5 (21.2)	-18.0 (0.09)
66784	NGC7059	SBc	64	12.43 (0.27)	0.14	0.33 (0.11)	1718.7 (21.2)	339.9 (21.2)	-20.1 (0.30)
54097	NGC5861	SBc	64.9	12.46 (0.13)	0.47	0.34 (0.09)	1850.2 (21.2)	426.8 (21.2)	-20.5 (0.17)
68618	IC5201	SBc	65.9	11.95 (1.15)	0.05	0.36 (0.22)	911.0 (21.2)	254.4 (21.2)	-19.2 (1.24)
6048	MCG-1-5-12	Sbc	66.7	15.21 (0.27)	0.12	0.34 (0.07)	1924.0 (21.2)	219.5 (21.2)	-17.5 (0.36)
68199	NGC7218	SBc	67	12.50 (0.19)	0.14	0.37 (0.06)	1644.2 (21.2)	326.8 (21.2)	-20.0 (0.32)
67920	ESO532-14	SBc	68.9	15.05 (0.24)	0.11	0.40 (0.07)	1694.5 (21.2)	199.5 (21.2)	-17.5 (0.25)

		LEDA Supplied					Measured		
PCG	Name	Morphology	Inclination	Apparent Magnitude	Galactic Extinction	Log a/b	Centre Velocity	Line Width	Absolute Magnitude
32044	NGC3361	SBc	69	13.41 (0.06)	0.14	0.39 (0.13)	1907.3 (21.2)	287.7 (21.2)	-19.4 (0.17)
38346	NGC4094	SBc	72.5	12.51 (0.22)	0.24	0.45 (0.05)	1424.6 (21.2)	332.1 (21.2)	-19.9 (0.25)
8320	ESO298-15	SBc	73.5	14.16 (0.30)	0.08	0.48 (0.07)	1411.4 (21.2)	213.7 (21.2)	-18.1 (0.34)
42123	ESO442-13	SBc	76.2	13.65 (0.39)	0.31	0.53 (0.10)	1509.8 (21.2)	241.0 (21.2)	-19.1 (0.43)
16983	ESO423-2	SBc	77.9	13.14 (0.20)	0.12	0.57 (0.07)	1455.8 (21.2)	267.9 (21.2)	-19.4 (0.24)
12916	NGC1337	SBc	79.3	12.53 (0.37)	0.29	0.59 (0.05)	1230.8 (21.2)	304.0 (21.2)	-19.9 (0.38)
8232	IC210	Sbc	80.1	13.95 (0.18)	0.1	0.55 (0.06)	1934.3 (21.2)	327.1 (21.2)	-19.1 (0.21)
46535	NGC5088	Sbc	81.6	12.88 (0.18)	0.23	0.58 (0.07)	1426.8 (21.2)	286.7 (21.2)	-19.6 (0.22)
627	NGC7	SBc	86.7	14.26 (0.48)	0.06	0.67 (0.13)	1474.1 (21.2)	204.9 (21.2)	-18.4 (0.51)
68305	ESO146-14	SBc	90	14.70 (0.21)	0.18	0.95 (0.20)	1672.6 (21.2)	199.4 (21.2)	-18.8 (0.26)
7244	ESO477-16	Sbc	90	14.92 (0.20)	0.07	0.87 (0.15)	1814.4 (21.2)	252.5 (21.2)	-18.3 (0.23)
66836	NGC7064	SBc	90	13.25 (0.50)	0.06	0.76 (0.04)	849.7 (21.2)	205.9 (21.2)	-18.3 (0.51)
2526	ESO540-16	SBc	90	14.49 (0.11)	0.09	0.91 (0.09)	1542.5 (21.2)	221.5 (21.2)	-18.7 (0.16)
67045	NGC7090	SBc	90	11.30 (0.10)	0.1	0.77 (0.08)	826.9 (21.2)	288.9 (21.2)	-20.3 (0.14)
11851	IC1898	SBc	90	13.74 (0.53)	0.1	0.77 (0.07)	1304.1 (21.2)	284.7 (21.2)	-18.9 (0.53)
52802	MCG-2-38-10	SBcd	51.2	16.00 (0.10)	0.35	0.20 (0.04)	1957.6 (21.2)	240.8 (21.2)	-16.8 (0.22)
12390	IC1914	SBcd	56.6	13.61 (0.71)	0.09	0.25 (0.07)	1009.5 (21.2)	319.8 (21.2)	-17.6 (0.72)
1284	ESO28-14	SBcd	63.5	16.39 (0.33)	0.24	0.33 (0.10)	1768.8 (21.2)	172.8 (21.2)	-16.3 (0.37)
16517	NGC1744	SBcd	66	11.70 (0.23)	0.18	0.36 (0.05)	734.9 (21.2)	252.9 (21.2)	-19.1 (0.27)
17567	ESO120-12	SBcd	67.8	13.52 (0.27)	0.33	0.27 (0.17)	1329.8 (21.2)	175.2 (21.2)	-18.5 (0.37)
14936	ESO550-24	SBcd	69.7	12.94 (0.68)	0.1	0.42 (0.08)	885.1 (21.2)	220.2 (21.2)	-18.3 (0.68)
70697	ESO407-9	SBcd	72.3	14.45 (0.46)	0.09	0.47 (0.07)	1554.7 (21.2)	282.6 (21.2)	-18.1 (0.47)
11984	ESO116-12	SBcd	78.3	13.21 (0.13)	0.1	0.59 (0.11)	1155.0 (21.2)	296.6 (21.2)	-18.9 (0.19)
16199	ESO361-15	SBcd	82.4	13.72 (0.85)	0.09	0.68 (0.14)	1160.5 (21.2)	242.8 (21.2)	-18.5 (0.85)
11595	ESO248-2	SBcd	82.5	14.26 (0.13)	0.06	0.69 (0.04)	1356.4 (21.2)	265.6 (21.2)	-18.3 (0.13)

		LEDA Supplied					Measured		
PCG	Name	Morphology	Inclination	Apparent Magnitude	Galactic Extinction	Log a/b	Centre Velocity	Line Width	Absolute Magnitude
2805	MCG-2-3-16	SBcd	90	14.23 (0.25)	0.15	0.82 (0.09)	1332.2 (21.2)	194.6 (21.2)	-18.6 (0.25)
66445	ESO107-16	SBcd	90	14.99 (0.11)	0.19	0.81 (0.07)	1763.8 (21.2)	192.7 (21.2)	-18.5 (0.11)
2445	ESO79-5	SBcd	90	14.52 (0.45)	0.09	0.42 (0.12)	1701.8 (21.2)	212.6 (21.2)	-18.1 (0.46)
65603	IC5052	SBcd	90	11.67 (0.25)	0.22	0.88 (0.12)	578.7 (21.2)	238.3 (21.2)	-19.5 (0.25)
16911	NGC1853	SBcd	90	13.51 (0.20)	0.08	0.49 (0.04)	1403.3 (21.2)	229.4 (21.2)	-18.8 (0.22)
46233	ESO444-2	SBd	48.4	14.94 (0.11)	0.31	0.14 (0.04)	1619.6 (21.2)	155.7 (21.2)	-17.3 (0.31)
45195	MCG0-33-28	SBd	49.4	14.74 (0.24)	0.13	0.14 (0.06)	1344.8 (21.2)	205.6 (21.2)	-16.9 (0.49)
3671	NGC337A	SBd	53.2	13.38 (0.90)	0.44	0.16 (0.05)	1063.1 (21.2)	157.0 (21.2)	-18.1 (0.91)
35705	MCG0-30-11	SBd	57	14.96 (0.67)	0.15	0.19 (0.06)	1588.1 (21.2)	211.3 (21.2)	-17.2 (0.71)
16236	ESO485-21	SBd	58.6	14.33 (0.73)	0.14	0.20 (0.17)	1363.2 (21.2)	137.4 (21.2)	-17.5 (0.81)
68253	ESO288-49	SBd	60.8	14.60 (0.86)	0.07	0.21 (0.08)	1941.5 (21.2)	224.0 (21.2)	-17.9 (0.88)
1440	ESO150-5	SBd	61.2	15.00 (1.27)	0.08	0.22 (0.09)	1423.8 (21.2)	149.5 (21.2)	-16.9 (1.28)
5764	ESO13-16	SBd	61.7	13.04 (0.19)	0.31	0.22 (0.05)	1742.5 (21.2)	210.1 (21.2)	-19.5 (0.29)
47102	ESO444-37	SBd	63.8	14.91 (0.20)	0.26	0.24 (0.06)	1876.6 (21.2)	210.4 (21.2)	-17.8 (0.32)
72957	ESO12-10	SBd	65.2	14.75 (0.27)	0.58	0.25 (0.16)	1902.4 (21.2)	287.1 (21.2)	-18.3 (0.45)
30041	IC600	SBd	69.9	14.03 (0.41)	0.15	0.28 (0.05)	1303.6 (21.2)	227.0 (21.2)	-17.8 (0.41)
71881	ESO347-29	SBd	70.7	14.32 (0.80)	0.08	0.29 (0.06)	1551.5 (21.2)	249.5 (21.2)	-17.9 (0.82)
13931	ESO54-21	SBd	71.7	13.06 (0.26)	0.22	0.30 (0.07)	1406.4 (21.2)	264.2 (21.2)	-19.1 (0.31)
3543	ESO541-5	SBd	71.9	15.58 (0.21)	0.09	0.30 (0.05)	1943.2 (21.2)	190.8 (21.2)	-17.1 (0.22)
9273	ESO479-4	SBd	74.6	12.78 (0.09)	0.08	0.32 (0.06)	1497.0 (21.2)	242.3 (21.2)	-19.4 (0.20)
64181	IC4951	SBd	90	13.91 (0.20)	0.17	0.82 (0.14)	810.1 (21.2)	159.6 (21.2)	-17.9 (0.22)
70089	NGC7412A	SBd	90	14.82 (0.66)	0.04	0.62 (0.31)	919.0 (21.2)	144.5 (21.2)	-16.8 (0.78)
800	ESO293-45	SBd	90	15.11 (0.23)	0.05	0.62 (0.10)	1459.4 (21.2)	207.4 (21.2)	-17.5 (0.23)
68201	ESO601-25	SBd	90	14.66 (0.21)	0.11	0.50 (0.04)	1711.8 (21.2)	172.2 (21.2)	-18.2 (0.21)
5329	MCG-1-4-42	SBd	90	15.26 (0.29)	0.14	0.39 (0.10)	1971.6 (21.2)	177.8 (21.2)	-17.7 (0.31)

		LEDA Supplied					Measured		
PCG	Name	Morphology	Inclination	Apparent Magnitude	Galactic Extinction	Log a/b	Centre Velocity	Line Width	Absolute Magnitude
13154	ESO482-5	SBd	90	15.23 (0.21)	0.11	0.78 (0.10)	1896.6 (21.2)	183.1 (21.2)	-18.3 (0.21)
14475	NGC1518	SBd	90	12.26 (0.12)	0.21	0.41 (0.10)	921.0 (21.2)	231.9 (21.2)	-19.1 (0.15)
72443	ESO149-1	SBd	90	13.45 (0.43)	0.07	0.71 (0.09)	1890.7 (21.2)	246.0 (21.2)	-19.9 (0.43)
9962	ESO115-21	SBd	90	13.07 (0.19)	0.11	0.86 (0.08)	512.2 (21.2)	172.9 (21.2)	-17.7 (0.21)
34691	ESO570-19	Sc	57.6	14.37 (0.13)	0.18	0.25 (0.07)	1316.5 (21.2)	259.7 (21.2)	-17.5 (0.24)
12285	NGC1292	Sc	67	12.79 (0.11)	0.08	0.36 (0.06)	1352.7 (21.2)	288.0 (21.2)	-19.2 (0.15)
57924	NGC6118	Sc	68.4	12.30 (0.23)	0.68	0.39 (0.05)	1551.2 (21.2)	403.4 (21.2)	-20.6 (0.25)
3980	NGC406	Sc	68.7	13.11 (0.18)	0.1	0.39 (0.05)	1492.4 (21.2)	302.4 (21.2)	-19.1 (0.21)
70304	NGC7456	Sc	72.8	12.43 (0.21)	0.04	0.47 (0.04)	1186.9 (21.2)	273.5 (21.2)	-19.4 (0.26)
17042	NGC1892	Sc	76.5	12.81 (0.08)	0.37	0.53 (0.05)	1340.5 (21.2)	277.3 (21.2)	-19.7 (0.12)
701	NGC24	Sc	80.8	12.14 (0.17)	0.08	0.59 (0.12)	543.5 (21.2)	248.6 (21.2)	-18.2 (0.22)
8673	IC217	Sc	83.6	14.32 (0.64)	0.1	0.67 (0.09)	1878.2 (21.2)	273.1 (21.2)	-18.9 (0.64)
69539	NGC7361	Sc	83.7	12.82 (0.10)	0.07	0.62 (0.07)	1246.4 (21.2)	256.1 (21.2)	-19.4 (0.10)
65960	IC5078	Sc	84.1	13.58 (0.07)	0.32	0.65 (0.12)	1455.9 (21.2)	300.7 (21.2)	-19.3 (0.15)
15749	ESO157-49	Sc	85.4	14.36 (0.09)	0.03	0.66 (0.04)	1654.3 (21.2)	264.3 (21.2)	-18.5 (0.09)
71889	ESO605-15	Sc	90	16.40 (0.12)	0.12	0.77 (0.12)	1538.9 (21.2)	112.2 (21.2)	-16.6 (0.14)
11016	ESO356-18	Sc	90	15.12 (0.26)	0.09	0.68 (0.08)	1459.0 (21.2)	233.3 (21.2)	-17.5 (0.27)
68726	ESO467-51	Sc	90	14.70 (0.18)	0.08	0.94 (0.12)	1801.8 (21.2)	224.8 (21.2)	-18.8 (0.19)
14190	NGC1495	Sc	90	13.48 (0.22)	0.06	0.71 (0.05)	1278.3 (21.2)	245.6 (21.2)	-18.9 (0.22)
13926	ESO482-46	Sc	90	13.74 (0.52)	0.05	0.82 (0.07)	1523.4 (21.2)	286.8 (21.2)	-19.2 (0.52)
17433	IC2135	Sc	90	13.20 (0.30)	0.17	0.78 (0.09)	1300.0 (21.2)	296.8 (21.2)	-19.5 (0.31)
72178	ESO292-14	Sc	90	13.83 (0.32)	0.04	0.88 (0.08)	1478.7 (21.2)	280.1 (21.2)	-19.2 (0.33)
47394	NGC5170	Sc	90	12.10 (0.16)	0.34	0.84 (0.07)	1489.6 (21.2)	545.2 (21.2)	-21.1 (0.18)
36887	UGC6780	Scd	67.2	15.28 (0.24)	0.09	0.38 (0.16)	1702.3 (21.2)	283.8 (21.2)	-17.3 (0.48)
3062	MCG-1-3-27	Scd	72.7	15.11 (0.27)	0.25	0.47 (0.04)	1398.9 (21.2)	191.6 (21.2)	-17.3 (0.27)

		LEDA Supplied					Measured		
PCG	Name	Morphology	Inclination	Apparent Magnitude	Galactic Extinction	Log a/b	Centre Velocity	Line Width	Absolute Magnitude
35271	MCG-1-29-23	Scd	73.3	15.33 (0.35)	0.2	0.49 (0.07)	962.2 (21.2)	133.1 (21.2)	-16.3 (0.36)
71501	ESO240-4	Scd	86.1	15.48 (0.15)	0.06	0.76 (0.15)	1571.4 (21.2)	119.3 (21.2)	-17.5 (0.17)
48976	ESO577-38	Scd	90	16.68 (0.20)	0.39	0.97 (0.30)	1875.5 (21.2)	150.3 (21.2)	-17.4 (0.37)
29086	MCG-1-26-12	Scd	90	14.58 (0.13)	0.17	0.99 (0.05)	653.7 (21.2)	154.5 (21.2)	-17.0 (0.14)
28136	UGC5245	Sd	90	15.98 (0.23)	0.19	0.85 (0.10)	1387.8 (21.2)	188.6 (21.2)	-17.1 (0.23)
36551	MCG-1-30-27A	Sd	90	14.64 (0.18)	0.11	0.44 (0.06)	1615.5 (21.2)	218.5 (21.2)	-17.9 (0.19)

Table 2: Sample Galaxy Data. Where available standard deviations are quoted in parentheses. The measured line width has been corrected for inclination.

References

[1] R. B. Tully and J. R. Fisher. A new method of determining distances to galaxies. *Astronomy and Astrophysics*, 54:661–673, February 1977.

[2] S. Sakai, J. R. Mould, S. M. G. Hughes, J. P. Huchra, L. M. Macri, R. C. Kennicutt, B. K. Gibson, L. Ferrarese, W. L. Freedman, M. Han, H. C. Ford, J. A. Graham, G. D. Illingworth, D. D. Kelson, B. F. Madore, K. Sebo, N. A. Silbermann, and P. B. Stetson. The Hubble Space Telescope Key Project on the Extragalactic Distance Scale. XXIV. The Calibration of Tully-Fisher Relations and the Value of the Hubble Constant. *Astrophysical Journal*, 529:698–722, February 2000.

[3] Michael Pierce. Tully-fisher relation. In *Encyclopedia of Astronomy and Astrophysics*. Nature Publishing Group, 2001.

[4] A. Sandage and G. A. Tammann. Steps toward the Hubble constant. IV - Distances to 39 galaxies in the general field leading to a calibration of the galaxy luminosity classes and a first hint of the value of H sub 0. *Astrophysical Journal*, 194:559–568, December 1974.

[5] R. B. Tully, M. J. Pierce, J. Huang, W. Saunders, M. A. W. Verheijen, and P. L. Witchalls. Global Extinction in Spiral Galaxies. *Astronomical Journal*, 115:2264–2272, June 1998.

[6] Roger A. Kaufmann, William J. Freedman. *Universe*. W. H. Freeman and Company, 5th edition, 1999.

[7] D. G. Barnes, L. Staveley-Smith, W. J. G. de Blok, T. Oosterloo, I. M. Stewart, A. E. Wright, G. D. Banks, R. Bhathal, P. J. Boyce, M. R. Calabretta, M. J. Disney, M. J. Drinkwater, R. D. Ekers, K. C. Freeman, B. K. Gibson, A. J. Green, R. F. Haynes, P. te Lintel Hekkert, P. A. Henning, H. Jerjen, S. Juraszek, M. J. Kesteven, V. A. Kilborn, P. M. Knezek, B. Koribalski, R. C. Kraan-Korteweg, D. F. Malin, M. Marquarding, R. F. Minchin, J. R. Mould, R. M. Price, M. E. Putman, S. D. Ryder, E. M. Sadler, A. Schröder, F. Stootman, R. L. Webster, W. E. Wilson, and T. Ye. The Hi Parkes All Sky Survey: southern observations, calibration and robust imaging. *Monthly Notices of the Royal Astronomical Society*, 322:486–498, April 2001.

[8] G. Paturel, L. Bottinelli, and L. Gouguenheim. An extragalactic database V. Conversion of apparent B magnitudes to a standard system. *Astronomy and Astrophysics*, 286:768–774, June 1994.

[9] D. J. Schlegel, D. P. Finkbeiner, and M. Davis. Maps of Dust Infrared Emission for Use in Estimation of Reddening and Cosmic Microwave Background Radiation Foregrounds. *Astrophysical Journal*, 500:525+, June 1998.

[10] A. M. Garcia. General study of group membership. II - Determination of nearby groups. *Astronomy and Astrophysics, Supplement*, 100:47–90, July 1993.

[11] Ben Mathiesen. Internet `http://www.physics.lsa.umich.edu/IP-LABS/Errordocs/properr.html`, July 1997.